Research on the Thermo-Physical Properties of Corncob Residues as Gasification Feedstock and Assessment for Characterization of Corncob Ash from Gasification

Xiwen Yao,[a] Kaili Xu,[a,*] and Yu Liang [b]

Harnessing energy from biomass is environmentally friendly because of the essentially zero net CO_2 impact. As a common agricultural byproduct, corncobs are abundant in quantity. This study was carried out to examine the thermo-physical properties of corncobs and characterize the properties of corncob ash produced from gasification, in order to provide a basis for transforming it into value-added products. The results showed that the pyrolysis of corncobs followed a three-step, stepwise mechanism. Activation energies calculated by the Coats-Redfern method at heating rates of 5, 10, and 20 °C/min were 79.08, 76.73, and 75.78 $kJ \cdot mol^{-1}$, respectively, implying that the corncobs could be decomposed easily at high heating rates. The emissions of CO, CO_2, CH_4, H_2, H_2O, and O_2 during pyrolysis corresponded well with thermal curves. Corncob ash could be a good fertilizer because of its high contents of K, P, and Ca. The high SiO_2 content makes the corncob ash suitable for ceramics and blended cement concrete. Sylvite (KCl) and quartz (SiO_2) were the two major crystal phases in the corncob ash. Relatively large particles of unburnt carbon residues in the ash indicated that low-cost adsorbent could be developed from these carbon residues.

Keywords: Pyrolysis; Gasification; Corncob; Kinetics; Corncob ash; Ash characterization

*Contact information: a: School of Resources and Civil Engineering, Northeastern University, Shenyang 110819, PR China; b: College of Information Science and Engineering, Northeastern University, Shenyang 110819, PR China; *Corresponding author: neu_kailixu@126.com*

INTRODUCTION

In recent years, because of the damage to natural resources and the unrestrained usage of limited fossil fuels, several crucial issues, such as global warming, energy shortage, environmental pollution, and extreme climate events have appeared more frequently than before (Zhang *et al*. 2016). For this reason, increasing attention has been drawn towards the exploitation of new sustainable fuel sources. Solar energy can be converted into chemical energy by plants, which is stored in the structural components of biomass (Kumar *et al*. 2008). Therefore, as a renewable source of energy, biomass waste is one of the key potential energy resources to satisfy the increasing energy needs while being environmentally benign (Mazlan *et al*. 2015).

With an annual top production among all agricultural grains, corn plays a significant role in the agricultural world, with an enormous amount of byproducts, such as corn straw (CS) and corncobs (CC) (Chyang *et al*. 2012). The low heating value (LHV) of CC is much higher than that of CS, indicating that CC are more suitable to be used as a biomass fuel than as a fertilizer (Avila-Segura *et al*. 2011). Currently, harnessing energy from biomass mainly focuses on the thermo-chemical processes, such as combustion, gasification, liquefaction, *etc*. (McKendry 2002). Among these processes, gasification has

attracted more attention because of its conversion of biomass into synthesis gas. The synthesis gas can be directly used for engine fuels or converted into liquid fuels by different processes (Kumar *et al*. 2009; Pan and Eberhardt 2011).

Pyrolysis, as a promising thermo-chemical conversion route, is a subcategory of gasification, and it plays an important role in biomass conversion (Yang *et al*. 2007). The development of a mathematical model predicting the qualities of gaseous products in the processes of gasification and pyrolysis requires the knowledge of the thermal pyrolysis kinetics of biomass (Kumar *et al*. 2008). Researchers have carried out numerous studies on the thermo-physical characterization of different biomass feedstocks, such as corn stover (Kumar *et al*. 2008), cotton stalk (Munir *et al*. 2009; Sun *et al*. 2010; Zhang *et al*. 2016), pine sawdust (Gao *et al*. 2013), apple pomace (Baray *et al*. 2014), sugar cane bagasse (Munir *et al*. 2009; Meng *et al*. 2013), hardwood residues (Mazlan *et al*. 2015), wood lignin (Liu *et al*. 2008), soybean stalk and sorghum stalk (Zhang *et al*. 2016), *etc*. In addition, the composition and content of the main biomass component can significantly affect the thermal decomposition during the biomass pyrolysis (Zhang *et al*. 2016). Yang *et al*. (2007) and Wu *et al*. (2013) revealed the pyrolysis characteristics of the main biomass components, such as hemicellulose, cellulose, and lignin for hydrogen production. Such research has shown that the pyrolysis behaviors of various biomasses are quite different, which can be mainly attributed to their chemical components. Particularly, in previous studies, many experimental investigations have been conducted to obtain the thermal efficiency of a combustion system using CC residues (Lin *et al*. 1995; Youssef *et al*. 2009). The research conducted by Tippayawong *et al*. (2006) further established that CC was suitable for burning as an alternative fuel instead of serving as a fertilizer by using the heat from CC combustion in a combustor for tobacco drying. Thus, on account of the abundant supply of CC in the world, more research attention should be paid on the new thermo-chemical technologies for converting CC to biomass energy forms.

Additionally, among the thermo-chemical conversion techniques commonly used in the countryside, biomass gasification and pyrolysis not only can exert a great influence on reducing the environmental pollutions caused by direct combustion of biomass, but also they can improve the thermal efficiency of biomass conversion (Yao *et al*. 2016). However, the inorganic minerals left after the thermo-chemical process are biomass ash, and they are generally regarded as waste materials of little or no value, the disposal of which is expensive and not environmentally friendly. Thus, from an economic and environmental point of view, it is quite meaningful to explore the properties of biomass ash.

As a natural lignocellulosic polymer material, the massive CC surpluses around the world are good precursor materials for further use in several industrial processes such as bioenergy production, thermal pyrolysis, and composites fabrication. Although there are a variety of studies that have focused on the thermo-physical properties of various biomass, and different values have been obtained due to different kinetic method adopted to calculate the activation energy, few studies have looked into the non-condensable gas analysis of the evolved chemical species during the pyrolysis of CC residues, which is significant for understanding the pyrolysis behaviors of CC and the reactions relevant to its decomposition process. It can also enhance the performance of bioenergy production by investigating the thermal decomposition of CC during the pyrolysis process.

Besides, it is fascinating that large amounts of corncob ash (CCA) can be generated from the thermo-chemical conversion of CC. To the best of the authors' knowledge, there have been few detailed studies on the performance properties of CCA obtained from gasification process or other thermo-chemical conversions (Adesanya and Raheem 2009;

Wang *et al*. 2012; Shim *et al*. 2015). From this fact it seems likely that understanding of the performance properties of the waste biomass ash is essential for transforming it into useful and profitable products. Hence, the objectives of this study were to determine the pyrolysis behaviors of CC by paying close attention to gas formation during the thermal decomposition of CC to facilitate its further utilization in bio-syngas production studies, and to characterize the properties of CCA to support analysis of its potential to be converted into ecofriendly and high value-added products.

EXPERIMENTAL

Biomass Samples and Thermogravimetric Analysis

Prior to the experiments, the CC samples were collected from the countryside of Shenyang, Liaoning province, northeast China. First, the raw biomass samples were dried at 105 °C ± 0.5 °C for 24 h in an oven. Then, the samples were ground and pulverized using a high-speed rotary cutting mill. Finally, they were sieved with a 100-mesh sieve. The materials that passed through the sieve (< 0.154 mm in size) were gathered in a closed container and kept for analysis. The particle size distribution of the prepared biomass feedstock are shown in Table 1. Table 2 presents the basic characterization of the pretreated CC residues, with each value being the mean value of three tests. The component analysis results of CC based on the literature data of the authors (Yao and Xu 2015) are listed in Table 3.

As a note, proximate analysis was done on an as-received basis, while ultimate analysis and low heating value (LHV) were done on a dry basis. The volatile matter, fixed carbon, and ash content were measured using a 5E-MACIII Infrared Speediness Coal Analyzer, China. The moisture was determined with a Sartorius Moisture Analyzer IMA 30. Ultimate analysis was analyzed quantitatively with a Vario MACRO Elemental Analyzer of Elementar, Germany. The LHV of CC was measured by means of an IKA Calorimeter System C2000. All the values in Table 2 presented a good reproducibility with the standard deviation less than 2.0%, and the precision of these measurements was 0.5%.

Table 1. Particle Size Distribution of Biomass Feedstock

D_{10} (μm)	D_{25} (μm)	D_{50} (μm)	D_{75} (μm)	D_{90} (μm)	D_{av} (μm)	S/V (m^2/ cm^3)
12.82	53.71	79.96	98.50	126.35	83.64	0.78

Notes: D_{10} stands for ash particle diameter below which the accumulated percentage is 10%; D_{25} stands for particle diameter below which the accumulated percentage is 25%, etc; D_{av} stands for the mean diameter; *S*/*V* stands for the ratio of the total surface area and volume of the particles.

Table 2. General Characterization of CC Residues

Proximate Analysis (wt.%)				Ultimate Analysis (wt.%)					LHV (MJ/kg)
Volatile Matter	Moisture	Fixed Carbon	Ash	C	H	O	N	S	
79.25	0.87	17.64	2.24	47.26	5.79	43.23	0.56	0.05	18.15

Table 3. Component Analysis of CC Residues

Cellulose (wt.%)	Hemicellulose (wt.%)	Lignin (wt.%)
47.60	32.00	16.40

The thermogravimetric analysis of the prepared CC materials was carried out in a sensitive thermal balance (NETZCH-STA449 F3, Selb, Germany) at heating rates of 5, 10, and 20 °C/min, up to a final temperature of 1200 °C. For the pyrolysis, high purity helium (99.99%) at a flow velocity of 30 mL/min was used as the carrier gas. The sensitivity was 1 μg and 0.01 °C, and about 5 mg of biomass samples were needed for each measurement. A quadrupole mass spectrometer (QMS 403D, Pfeiffer Vacuum Technology, Selb, Germany) coupled to the thermal balance was employed for gas evolution analysis.

Ash Preparation and Characterization Determination

In this study, the used ash materials were derived from the cyclone separator of a CC-sourced gasification plant in the Huangtukan Village of Shenyang, Liaoning Province, China. The gasification of CC was carried out in a downdraft fixed bed with an internal diameter of 1.03 m and a height (from the gasifier top to the grate) of 1.88 m. The gasification started with preheating of the bed by means of an external burner. Once the gasifier was heated up to 200 °C (temperature at the combustion zone in the inner wall of gasifier), air entered the gasifier with an equivalent ratio of 0.8, and the bio-syngas was mainly generated between 680 and 850 °C. The conveying system for bio-syngas could provide a maximum pressure of 20 kPa. This gasification plant had a maximum thermal input of 175 kW. The bio-syngas from biomass gasification was mainly composed of CO, CO_2, CH_4, and H_2, and this gasification plant could provide bio-syngas simultaneously for approximately 300 households for their cooking and warmth.

Figures 1(a)-(c) shows pictures of the gasification plant, the downdraft gasifier, and a scheme of the layout of this plant, respectively. As can be seen from Fig.1, this gasifier was followed by a gas cleaning and cooling system, which was equipped with a cyclone dust collector, a spray-dryer system, and a tar scrubber.

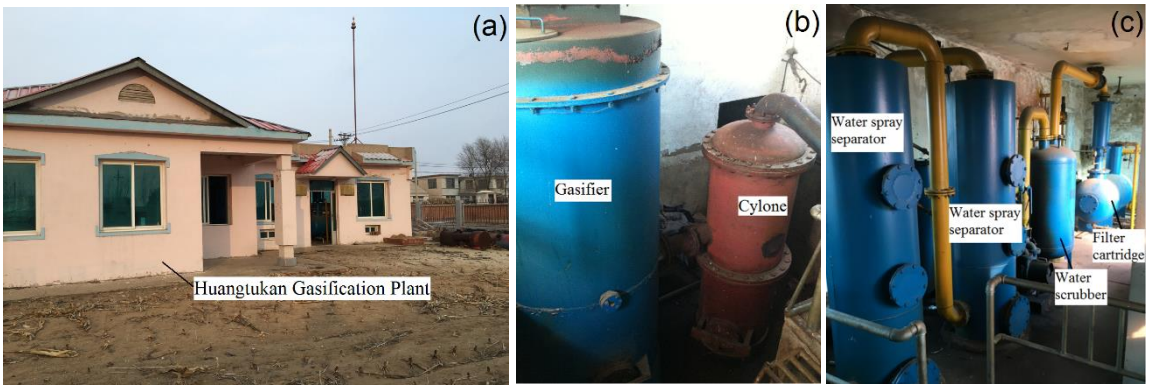

Fig. 1. Pictures of the gasification plant (a), the downdraft gasifier (b) and the scheme of the layout of this plant (c)

The collected ash materials were first smashed using a ball mill because of severe non-homogeneity, and then they were dried at 105 °C ± 0.5 °C for 24 h. Finally, these dried ash samples were sieved by a griddle with 100 meshes (0.154 mm) before experimental

analyses. Figures 2(a) and (b) show the appearance of the raw ash and the sieved ash powders, respectively. A laser particle size analyzer (LPSA) (Winner 3001, Jinan Micro-nano Particle Instrument Co., Jinan, China) was used to measure the particle size distribution of the raw CCA with a medium diameter of 136.72 μm (*i.e.*, D_{50}) (Table 4). The granularity analysis results determined by LPSA also revealed that the prepared CCA particles ranged in size from 1 to 150 μm with a medium diameter of 10.23 μm.

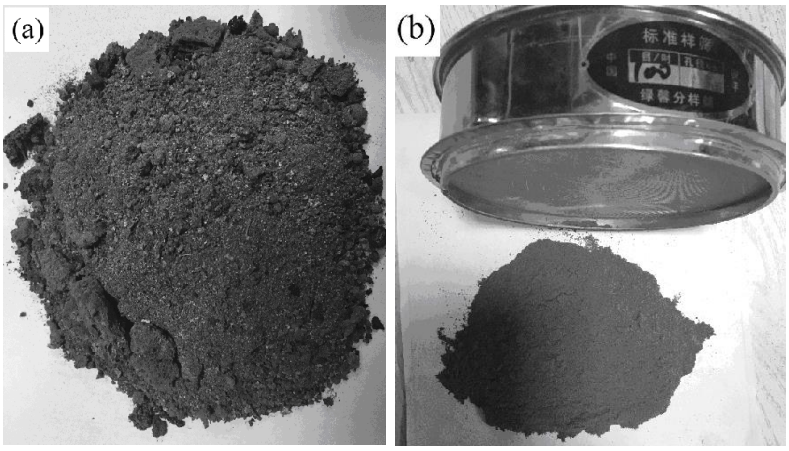

Fig. 2. Appearance of the raw ash materials (a) and the sieved ash powders (b)

Table 4. Particle Size Distribution of the Raw CCA Particles

D_{10} (μm)	D_{25} (μm)	D_{50} (μm)	D_{75} (μm)	D_{90} (μm)	D_{av} (μm)	S/V (m^2/ cm^3)
20.83	67.39	136.72	271.25	343.16	183.60	0.32

Notes: D_{10} stands for ash particle diameter below which the accumulated percentage is 10%; D_{25} stands for particle diameter below which the accumulated percentage is 25%, etc; D_{av} stands for the mean diameter; S/V stands for the ratio of the total surface area and volume of the particles.

The chemical composition of the CCA was obtained using X-ray fluorescence (XRF) (ZSX100e, Rigaku Co., Tokyo, Japan). The main crystalline minerals were qualitatively determined by an X-ray diffractometer (XRD) (X'Pert PRO, PANalytical B.V., Almelo, Netherlands).

Scanning electron microscopy (SEM) (Ultra Plus, Carl Zeiss Co. Ltd., Oberkochen, Germany) and energy dispersive X-ray (EDX) (Genesis, Edax DX-4) were carried out to acquire information on the morphological structure and elemental composition of the ash surface.

In addition, the above-mentioned thermogravimetric (TG) analyzer (NETZCH-STA449 F3, Selb, Germany) was also used to get weight loss data, and a differential thermal analyzer (DTA) was used to obtain the phase transition as a function of temperature. The results from the TG and DTA analysis performed on CCA samples could be found in the previously-published work of the authors, which widely presented this data (Yao and Xu 2016). In the cited paper the thermal characteristics of CCA from gasification process and combustion process were comparatively studied with TG and DTA instruments, respectively.

RESULTS AND DISCUSSION

Thermogravimetric Characterization of CC

Figure 3 exhibits the thermal curves obtained for the CC at the heating rates of 5, 10, and 20 °C/min under a helium atmosphere. The characteristic parameters determined from the TG and differential thermogravimetric (DTG) profiles under various heating rates are described in Table 5.

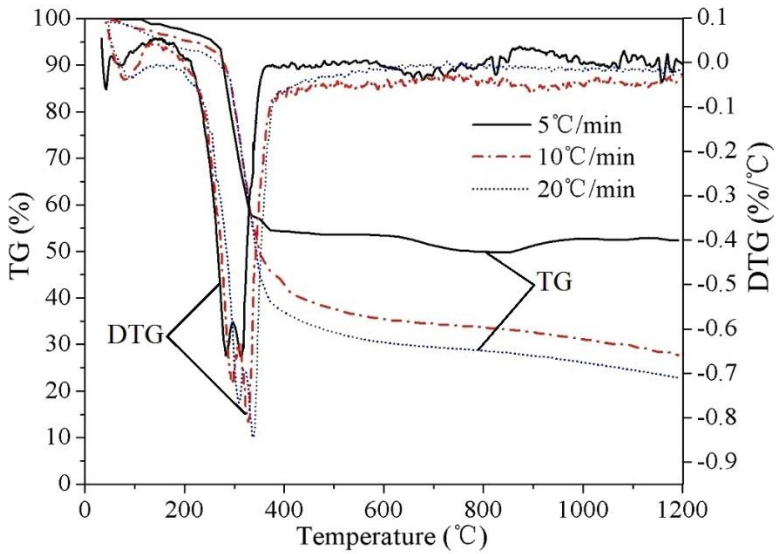

Fig. 3. Thermal curves of CC obtained at various heating rates

As can be observed from the TG curves in Fig. 3, the thermal decomposition of the CC followed an evident three-step, stepwise mechanism. The first weight loss (below 140 °C) started at approximately 70 °C, and it was mainly due to the evaporation of unbound moisture in the CC biomass. Moreover, as can be seen from the DTG curves in Fig. 3, the initial decomposition rates were quite slow. However, there was an obvious shoulder peak between 70 °C and 140 °C for all of the heating rates. Munir *et al*. (2009) suggested that the weight loss taking place around 100 °C was partly related to the beginning of the thermal pyrolysis of hemicellulose and lignin in biomass.

Table 5. Characteristic Parameters from the TG-DTG Curves

Heating Rate (β) (°C/min)	Starting Temp (T_s) (°C)	Peak Temp (T_{max}) (°C)	Final Temp (T_f) (°C)	Temperature of Full Width at Half Maximum ($\Delta T_{1/2}$) (°C)	Maximum Degradation Rate $(dw/dt)_{max}$ (%/°C)	Mean Degradation Rate $(dw/dt)_{mean}$ (%/°C)	Total Weight Loss (W_t) (%)
5	176.7	314.8	665.6	71.4	-0.679	-0.098	47.79
10	179.8	326.5	681.3	67.5	-0.796	-0.139	69.65
20	183.3	334.4	703.5	69.2	-0.881	-0.148	77.23

The major weight loss occurred beyond 140 °C and up to 420 °C, accompanied by two sharp peaks in the weight loss rate. The weight loss in this pyrolytic zone greatly

contributed to the total weight loss (approximately 80 wt.% to 90 wt.%), which was mostly due to the evolution of volatiles released from the thermal pyrolysis of the main components of biomass. Corncobs are mainly composed of cellulose, hemicellulose, and lignin, and it has been discovered that cellulose mostly decomposes within 277 to 427 °C, hemicellulose within 197 to 327 °C, and lignin within 277 °C to 527 °C (Du *et al*. 1990). Specifically, it can be observed from the DTG curves that the temperature corresponding to the maximum degradation rate tended to gradually shift towards a higher temperature zone with increasing heating rate. Finally, after 420 °C, a negligible weight loss was observed with a slow decomposition rate. The pyrolytic process was mostly complete at approximately 600 °C.

Based on the characteristic parameters shown in Table 5, the starting temperature (T_s), final temperature (T_f), and peak temperature (T_{max}) of the main weight loss, along with the maximum degradation rate $(dw/dt)_{max}$ and the mean weight loss rate $(dw/dt)_{mean}$, all increased remarkably with increasing heating rate. As it can be seen from Fig. 3, the maximum degradation rate tended to rise at faster heating rates. And with the increment of heating rate, the peak temperature (T_{max}) corresponding to the maximum degradation rate presented a tendency to shift to a higher temperature zone. In addition, the other two characteristic temperatures (T_s and T_f) also increased obviously with the increment of heating rate (Table 5). These results were mainly attributed to the fact that more thermal energy could be provided at a relatively faster heating rate, which promoted the thermal transmission nearby and within the CC materials (Baray *et al*. 2014).

In addition, when the heating rate was 5, 10, and 20 °C/min, the total weight loss (W_t) was 47.79%, 69.65%, and 77.23%, respectively. To a certain degree, this trend was opposite to the findings of previous research studies (Brachi *et al*. 2015; Baroni *et al*. 2016), and this was mainly attributed to the fact that during the pyrolysis the thermal cracking reaction in low temperature zone could be decreased obviously with the increment of heating rate, which facilitated the conversion of lignin and reduced the coke yield (Ferdous *et al*. 2001). Thus, a higher weight loss could be generated as the heating rate was increased. Besides, these results also indicated that the pyrolysis of CC at a relatively high heating rate could result in more complete decomposition, and thus, pyrolysis with a fast heating rate at low temperatures would be more suitable for biomass gasification in practice, basically consistent with the results of Cao *et al*. (2004).

As can be observed from Table 5, the final value of the weight loss at the heating rate of 5 °C/min was around 48 wt.%, which was much lower than the volatile content of CC (79.25 wt.%), although the biomass was heated up to a very high temperature (1200 °C). However, with the increment of heating rate, the total weight loss value increased remarkably, indicating that the CC could be completely decomposed to carbon residues at a relatively higher heating rate. Particularly, in case of 20 °C/min, the total weight loss value was up to 77.23 wt.%, which was very close to the volatile content of CC. Thus, these results further revealed that the heating rate can produce a significant impact on the evolution of volatile matters during the biomass pyrolysis. In other words, at a relatively lower heating rate, the volatile matters in biomass cannot achieve complete evolution, which can be confirmed by the MS profiles in the subsequent analyzes.

Parameters of Reaction Kinetics

The thermogravimetric data obtained from the various heating rates can be used for the determination of pyrolysis reaction kinetics. The integral Coats-Redfern method was employed for mathematical analysis, which has been successfully employed for investigations of the pyrolysis kinetic parameters (Liang and Kozinski 2000; Vamvuka *et al*. 2003; Sun *et al*. 2010). The degradation rate of biomass is defined as the equation of an Arrhenius type kinetic model, and the first-order-reaction-based Arrhenius theory is commonly employed in the kinetic analysis of pyrolysis (Rath and Staudinger 2001). The reaction rate constant k (s^{-1}) can be described based on the Arrhenius equation (Eq. 1),

$$k = A\exp\left(-\frac{E}{RT}\right) \quad (1)$$

where k is the reaction rate constant (s^{-1}), T is the thermodynamic temperature (K), R is the universal gas constant (8.314 $J\cdot K^{-1}\cdot mol^{-1}$), E represents the activation energy ($kJ\cdot mol^{-1}$), and A is the pre-exponential factor (s^{-1}). The degradation rate of the biomass was expressed by Eq. 2,

$$\frac{d\alpha}{dt} = k(1-\alpha) \quad (2)$$

where $d\alpha/dt$ denotes the rate of the process ($\%\cdot s^{-1}$), and α is the fractional conversion (%), which was defined by Eq. 3,

$$\alpha = (w_0 - w)/(w_0 - w_f) \quad (3)$$

where w_o, w_f, and w are the biomass weight (wt.%) at the start, at the end, and at a specific time t, respectively.

For a constant heating rate program, where the temperature is raised at a constant rate $\beta = dT/dt$, Eq. (2) can also be expressed as Eq. (4):

$$\frac{d\alpha}{1-\alpha} = \frac{k}{\beta}dT \quad (4)$$

The integration of Eq. 4 can be expressed as Eq. 5,

$$g(\alpha) = \int_0^\alpha \frac{d\alpha}{1-\alpha} = \frac{A}{\beta}\int_0^T \exp\left(-\frac{E}{RT}\right)dT \quad (5)$$

where $g(\alpha) = -\ln(1-\alpha)$.

Equation 5 was integrated by the integral Coats-Redfern method (Jiang *et al*. 2010) to yield Eq. 6,

$$\ln\frac{g(\alpha)}{T^2} = \ln\left(\frac{AR}{\beta E}\left[1-\frac{2RT}{E}\right]\right) - \frac{E}{RT} \quad (6)$$

where $g(\alpha)$ represents the function of kinetic mechanism in an integral type.

The $2RT/E$ term can be regarded as negligible, since it is far less than 1. Therefore, Eq. 6 was simplified to Eq. 7:

$$\ln\frac{g(\alpha)}{T^2} = \ln\frac{AR}{\beta E} - \frac{E}{RT} \quad (7)$$

The ln ($g(\alpha)/T^2$) term varied as $1/T$ with a slope of $-E/R$ linearly. These trends are displayed in Fig. 4.

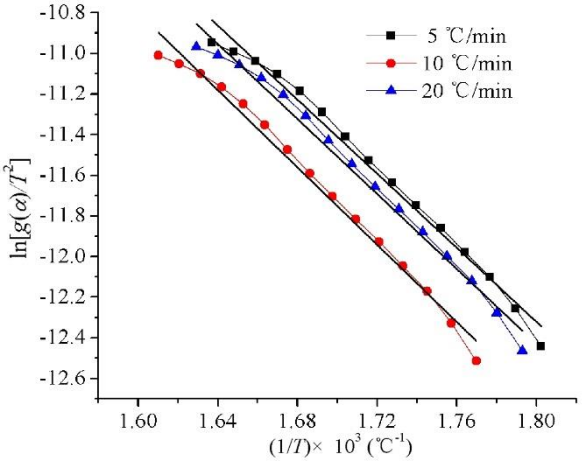

Fig. 4. Correlation between ln[$g(\alpha)/T^2$] and $1/T$

The pyrolysis kinetic parameters in the main pyrolysis stage, such as the activation energy (E) and pre-exponential factor (A), could be obtained by the above equations. The results are listed in Table 6. The points at which the temperatures were assigned for the temperature range adopted at different heating rates are defined in Fig. 5. The temperature range is precisely between the named T_1 and T_2 in Fig. 5.

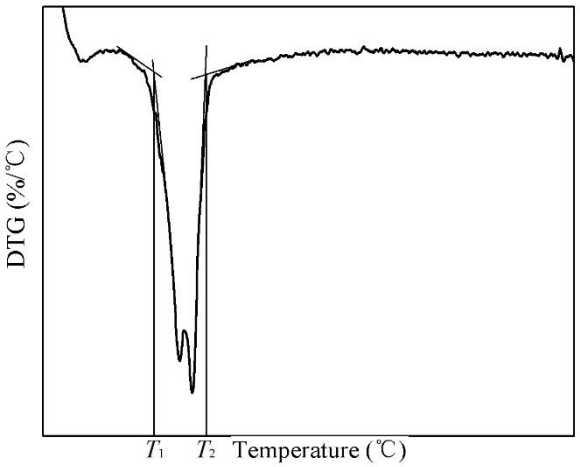

Fig. 5. Determination of points for the temperature range in Table 6

Table 6. Pyrolysis Kinetics of CC under Various Heating Rates

Heating Rate (°C /min)	Temperature Range (°C)	Fitting Equation	E (kJ·mol^{-1})	A (s^{-1})	R (Correlation)
5	271-350	Y=4.0856−9.1148X	79.08	4.518×10^4	0.99379
10	276-411	Y=4.4188−9.5116X	76.73	1.316×10^5	0.99381
20	281-423	Y=4.1820−9.2288X	75.78	2.015×10^5	0.99375

As shown in Table 6, the value of *E* calculated from the Coats-Redfern method under various heating rates was approximately 75 kJ·mol^{-1} to 80 kJ·mol^{-1}, which was much lower than that of coal (generally 120 kJ·mol^{-1} to 230 kJ·mol^{-1}) recorded in literature (Liang and Kozinski 2000). This result also indicated that the CC could be easily decomposed. Moreover, the activation energy decreased slowly with increasing heating rate, further implying that the energy required for pyrolysis under a high heating rate is slightly more than that of pyrolysis at a low heating rate.

As a note, in this study the kinetic activation energy was calculated from the original TGA data by using Coats-Redfern method, and the linear equations obtained at the different heating rate were fitted according to principles of least squares method. The calculated kinetic activation energy presented a good reproducibility with the standard deviation of < 0.5%, which further established the difference between the three activation energy data at the different heating rate.

The values of *R* corresponding to the linear fittings were greater than 0.99, implying a very strong linear relationship. The strong linear relationship between $\ln(g(\alpha)/T^2)$ and $1/T$ can also be clearly observed from Fig. 4. Thus, the pyrolytic process of CC can be explained in terms of the first-order-reaction with the Arrhenius theory, ignoring the moisture loss process.

Mass Spectrometry (MS) Evolution Profiles

The evolution profiles of typical, non-condensable gases (consisting primarily of CO, CO_2, CH_4, H_2, H_2O, and O_2) during the pyrolysis of CC residues were thoroughly investigated using the TG-MS method. The evolution profiles at various heating rates are shown in Fig. 6. Here, it is worth noting that quantitative ion measurements require that MS equipment be calibrated for the detected mass to charge ratios. Otherwise, although measurements of absolute intensity made of different spectra cannot be compared quantitatively, it can be useful to examine ratios of peak intensities.

As can be seen in Figs. 6(a)-(f), the main temperature zones for the evolution profiles of small-molecule gases and the temperatures relevant to their major emission peaks during the pyrolysis corresponded well with the thermal decomposition curves determined by TG analysis (Fig. 3). But, the ion intensities of the emission peaks for each of the same kind of gaseous product at different heating rates presented a remarkable difference. The evolution of CO took place without any distinct releasing peaks during the whole pyrolysis (Fig. 6(a)). Meng *et al*. (2013) suggested that CO was mostly evolved out from the cracking of carboxyl (C=O) and carbonyl (C–O–C) groups in the pyrolysis of hemicellulose, during the whole pyrolysis process, and in that of lignin above 600 °C. In addition, it should be noted that the CO intensity for a heating rate of 20 °C/min was much higher than that of the other heating rates (5 °C/min and 10 °C/min), indicating that the amount of CO released was high, and that it had a high intensity of ion current.

As for CO_2, it was produced in the largest amount between 230 and 500 °C, accompanied by an evident releasing peak at around 350 °C (Fig. 6(b)). Specifically, the CO_2 emission for the heating rate of 20 °C/min showed a small shoulder peak at around 480 °C, which can be clearly observed from the CO_2 release curve in case of 20 °C/min in Fig. 6(b). Beyond 500 °C, the evolution of CO_2 decreased quickly for all heating rates. According to Yang *et al*. (2007), at temperatures below 500 °C, the abundant presence of C=O chemical groups in the hemicellulose was suggested to favor the production of CO_2, while above 500 °C, the thermal pyrolysis of lignin contributed a small portion to it. In

addition, similar to the CO emission for 20 °C/min, the CO_2 emission for a heating rate of 20 °C/min was higher than those of lower heating rates.

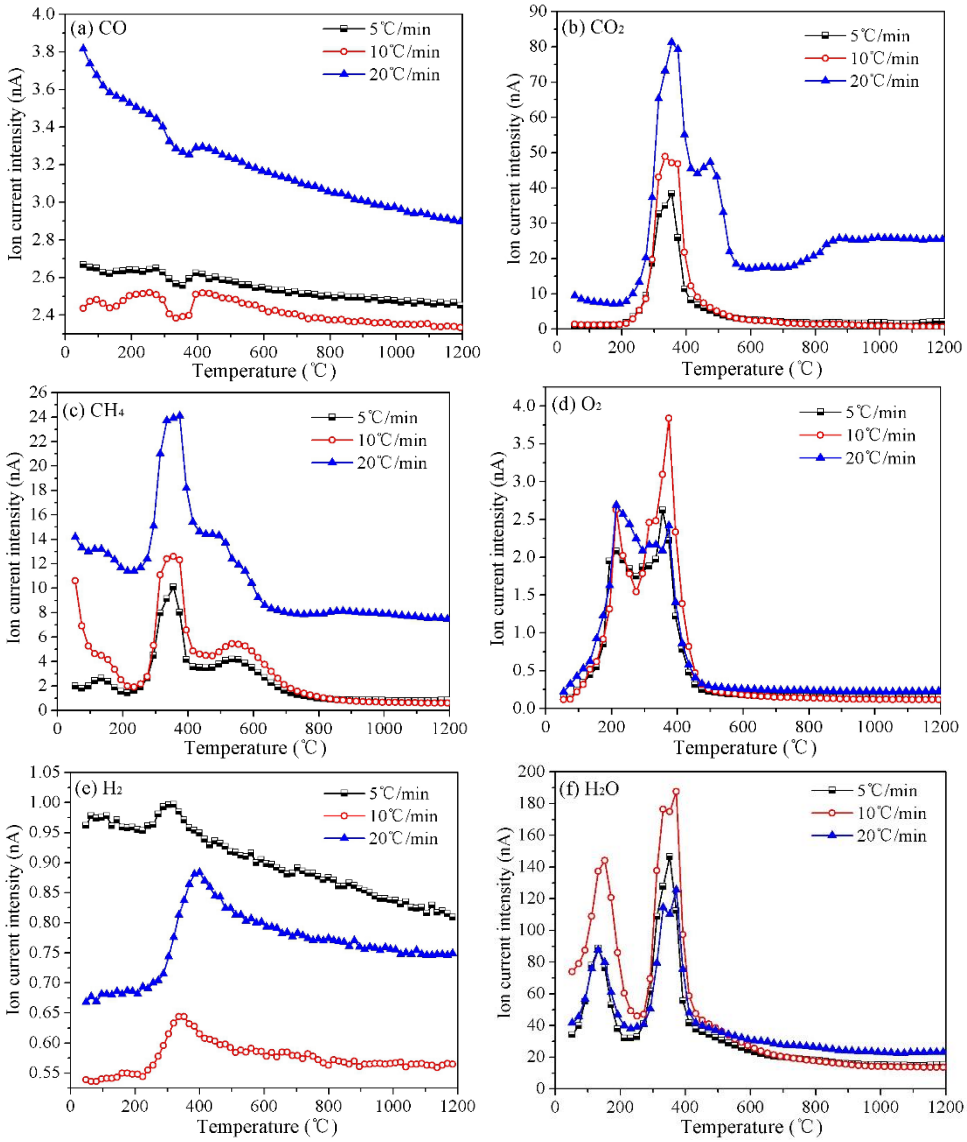

Fig. 6. MS ion intensity curves during the pyrolysis of CC under different heating rates

The releasing profiles of CH_4 showed a similar pattern to that of CO_2, except that its emission intensity was relatively lower (Fig. 6(c)). According to the literature (Liu *et al*. 2008), lignin is enriched with methoxyl-O-CH_3 chemical groups. Thus, it is to be inferred that the CH_4 was most likely produced through the cracking of methoxyl-O-CH_3 groups during the pyrolysis of lignin below 600 °C.

As can be seen from Fig. 6(d), the evolution of O_2 mainly occurred at low temperatures (< 400 °C), with two maximum peaks emerging at approximately 220 and 380 °C. At approximately 400 °C, the ion current intensity of O_2 reduced rapidly, and its emission was mostly complete at 450 °C. According to previous research (Li *et al*. 2001), the prevalent mechanism of the O_2 formation was mainly due to the elimination of O-acetyl groups that originally associated to the xylose units. As for methyl alcohols, it could be

generated by the thermal decomposition of methoxyl groups during the pyrolysis (Jensen *et al*. 1998). But, as one of the typical compounds from lignin pyrolysis, the O-methyl groups could be cracked to CO and H_2 at above 800 °C (Asmadi *et al*. 2011). Thus, the MS signal at m/z = 32 in this study mainly referred to the evolution of O_2.

Unlike CO_2, CH_4, and O_2, the evolution of H_2 covered a much wider temperature range, from approximately 200 °C to the final pyrolysis temperature (Fig. 6(e)), accompanied by one releasing peak within the range of 350 to 400 °C. Wu *et al*. (2013) suggested that the high H_2 emission could be obtained from the pyrolysis of cellulose and hemicellulose under 400 °C. After 400 °C, the H_2 emission showed a decreasing tendency, indicating that the lignin pyrolysis after 400 °C could also produce H_2.

The evolution of H_2O occurred early, at about 100 °C, and then rapidly increased with increasing pyrolysis temperature, reaching two emission peaks. The first peak occurred at approximately 130 °C, with a lower intensity, while the second peak occurred at approximately 350 °C, with a relatively higher intensity (Fig. 6(f)). The H_2O emission was mostly finished beyond 500 °C, and the emission within 100 to 500 °C was mostly from the evolution of bound water and bulk water, as well as crystallization water present in mineral substances (Gao *et al*. 2013). After 500 °C, the H_2O emission decreased remarkably with the elevated pyrolysis temperature.

Chemical and Phase Analysis of CCA

The chemical composition of the received CCA is depicted in Table 7. Figure 7 shows the direct-viewing XRD spectra of CCA. As a note, the studied CCA was mainly produced between 680 and 850 °C during the gasification of CC residues.

Table 7. Chemical Composition of CCA (wt. %)

K_2O	SiO_2	P_2O_5	CaO	MgO	Na_2O	Al_2O_3	Fe_2O_3	SO_3	MnO	TiO_2	Cl
31.50	28.39	7.53	9.72	1.66	4.99	3.58	1.10	2.52	0.09	0.21	8.71

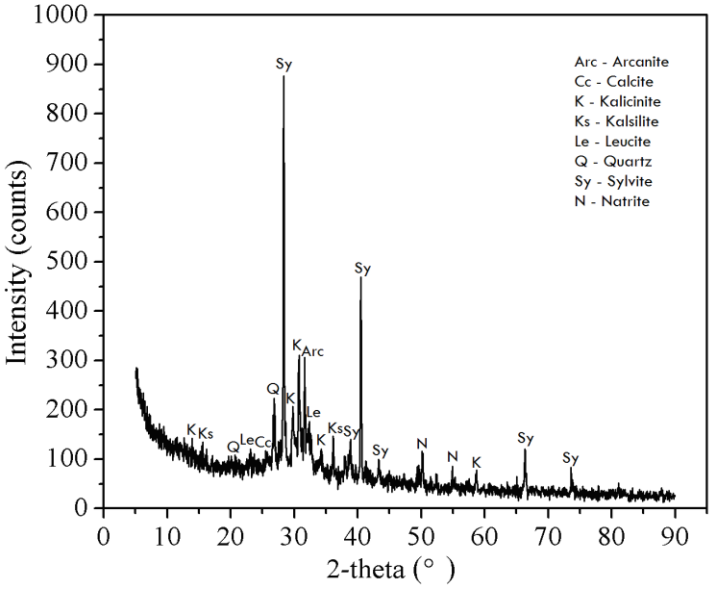

Fig. 7. X-ray diffraction patterns of CCA

As shown in Table 7, the CCA was primarily composed of K_2O, SiO_2, P_2O_5, CaO, and Cl. Lesser amounts of MgO, Na_2O, Al_2O_3, Fe_2O_3, SO_3, MnO, and TiO_2 were also detected. Particularly, the content of K_2O was quite high (31.50%). This high K_2O content could be a potentially existing problem, resulting in agglomeration of the bed material, as well as fouling and corrosion of the heat exchange surface, as seen in other biomass fuels (Liang and Kozinski 2000). Additionally, Vamvuka and Zografos (2004) demonstrated that chlorine could serve as a facilitator of alkali vaporization during the thermochemical process. Since the content of K_2O was the highest among those chemical components of CCA, it could be inferred that the content of the alkali metal element of K was also very high. Besides, the Cl content was up to 8.71%, which was higher than that of other biomass ashes (Vassilev *et al*. 2013). Hence, the appreciable contents of K and Cl could probably result in a serious vaporization of alkali metals in form of KCl.

SiO_2 was also prominent in the ash composition (28.39%), which indicated the potential of CCA to be utilized as a silica source for silicate ceramics production, similar to other biomass ashes recorded by Umamaheswaran and Batra (2008). Also, this result indicated that CCA with high silica content has good potential to be used for blended cement concrete production. But, it is worth considering that chlorides can be introduced to concrete made with CCA-blended cement, which is a critical problem for the reuse as a raw material in cement due to the primary corrosion of steel reinforcement caused by chloride attack. In a previous study (Adesanya and Raheem 2010), the influence of chloride attacks on the permeability of CCA-blended cement was evaluated. Besides, the reaction of blended cement mortar specimens with HCl acid water (mix proportions 1:1, 1:2, and 1:3 by weight) was also studied in-depth, and their results indicated that the incorporation of CCA could improve the resistance of concrete to chloride attack. In addition, Adesanya and Raheem (2009) reported that the CCA-blended cement concrete presented a long-term strength development.

The presence of CaO makes the resultant CCA possible for SO_2 capture (Abraham *et al*. 2013). In addition, as the XRF results presented, the CCA was devoid of toxic metals, implying its potential for clarification or separation in various industries. However, the utilization of CCA for clarification has not been explored until now, and it needs to be further investigated in future studies. These results were confirmed by XRD data (Fig. 7), which revealed the complex diffraction patterns caused by various phases emerging and potential peak overlapping. As the XRD pattern showed, potassium, commonly in the form of sylvite (KCl), and silica, in the form of quartz (SiO_2), were identified as the two major crystalline phases in the CCA. In addition, other forms of potassium, such as arcanite (K_2SO_4), kalsilite ($KAlSiO_4$), kalicinite ($KHCO_3$), and leucite ($KAlSi_2O_6$) were also identified. Sodium and calcium were mainly present in the forms of natrite (Na_2CO_3) and calcite ($CaCO_3$), respectively. From the point of view of nutrient elements (commonly K, P, and Ca) in biomass ash, the CCA, with its rich contents of K, P, and Ca, presents a good potential to be used as a soil amendment or a crude fertilizer.

SEM/EDX Analysis of CCA

The SEM images of CCA particles are shown in Figs. 8A-D, and the results of EDX analyses in spots a-d shown in Figs. 8A-D are illustrated in Figs. 8a-d, respectively. As a note, the EDX analyses were performed in a spot mode in which the beam was localized on a single area manually chosen within the field of view. The location is shown on the provided micrographs by a "+" for clearly identifying the exact spots of the SEM images which the EDX spectra refers to.

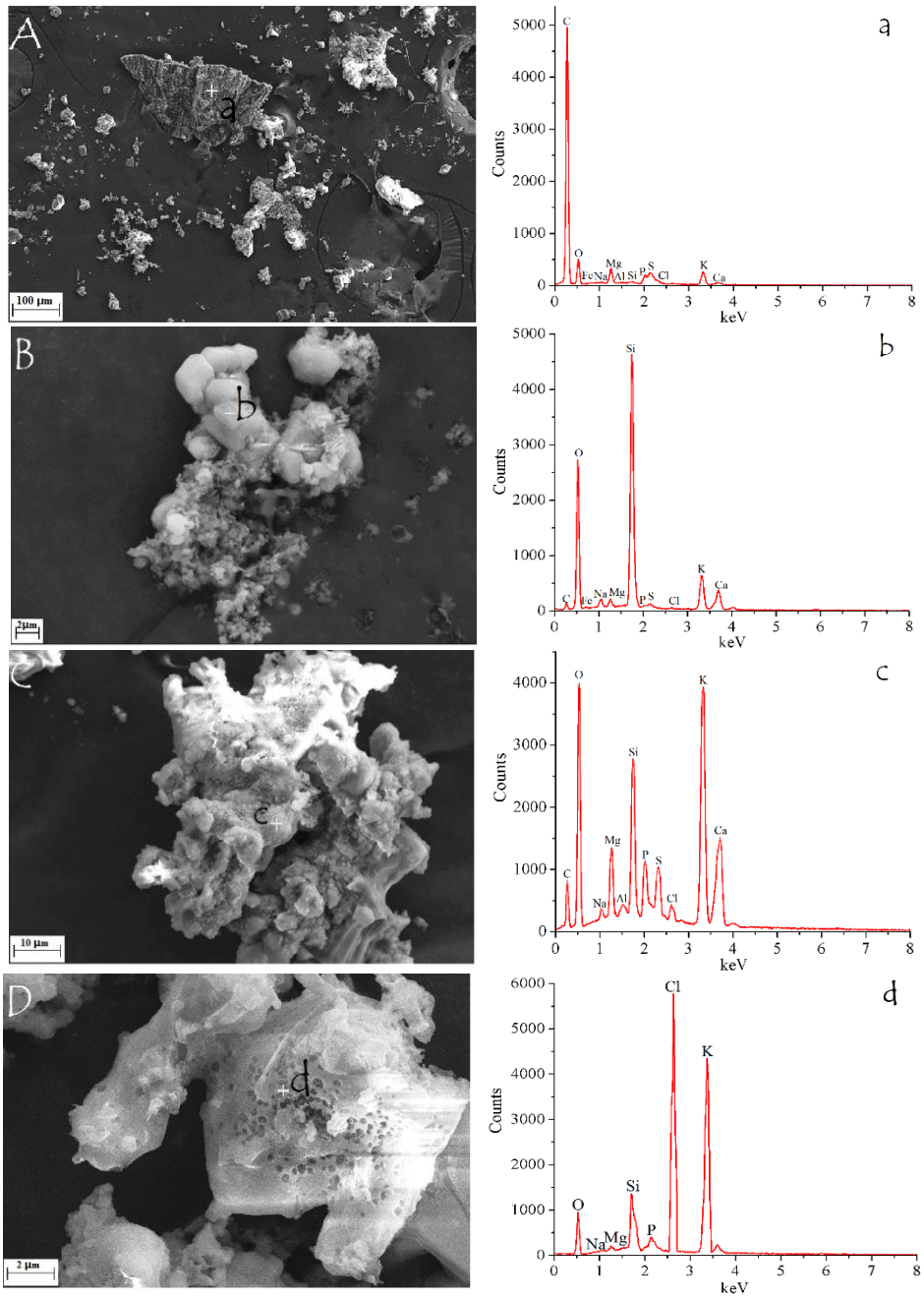

Fig. 8. SEM images and EDX spectra of the received CCA samples

The SEM analysis of the CCA revealed particles that were irregular and ranged in size from 1 to 150 μm (Fig. 8A). As can be seen from the SEM micrograph, some large, unburnt ash residues caused by inadequate conversion in the gasification process remained in the CCA. The EDX analysis of the unburnt ash surface revealed that the unburnt ash particles were mainly composed of carbon (Fig. 8a), indicating that these unburnt carbon residues could be potentially utilized as a precursor material for activated carbon production.

As can be seen from Fig. 8B, some quadrate crystalline phases were present in the CCA. The EDX analysis of the external surface of the crystalline phases showed that

silicon and oxygen were the two major elements (Fig. 8b). This result indicated that these crystalline phases could be identified as quartz, which was basically consistent with the XRD data (Fig. 7).

Figure 8C displays a typical agglomerate sample, the particle size of which is larger than 60 μm. Upon closer observation of this SEM image, many large voids can be clearly found throughout the agglomerate. The EDX analysis of the external surface of the agglomerate showed that the contents of alkali and alkali earth metals (such as K, Na, Ca, and Mg) were quite high (Fig. 8c), providing explicit evidence that the existence of alkali and alkali earth metals from CCA could result in the formation of the sticky surfaces of ash particles, which could then cause further agglomeration. Besides, these results were in accordance with those of other previous researches (Liang and Kozinski 2000; Chirone *et al*. 2004).

Figure 8D exhibits the interior details of a broken agglomerate sample. Upon examination of its interior, a porous structure with a large amount of pores on the internal surface can be clearly observed, which reveals the release of volatiles from the solid substrate during pyrolysis. To obtain the fraction of unburned carbon in the received ash, the method of density gradient centrifugation (DGC) was utilized for the separation of unburned carbon. The detailed procedures of DGC method could be found in previous literature (Maroto-Valer *et al*. 1999). The results indicated that the unburned carbon content in the received CCA in this study was up to approximately 20%, which made CCA suitable for use as a precursor material for the production of activated carbon. This result further verified that low-cost adsorbent could be developed from the carbon residues isolated from the CCA. The EDX analysis showed that the internal surface of this agglomerate sample was enriched with potassium and chlorine (Fig. 8d), suggesting that the emission of potassium was mostly in the form of KCl. In addition, this chloride could be gradually released from the inside of the biomass during pyrolysis, and then stay on the external surface of ash powders.

CONCLUSIONS

Thermogravimetric experiments of CC conducted in an inert atmosphere suggested that there were three evident stages of weight loss. Increasing heating rate appeared to increase the characteristic parameters of T_s, T_{max}, T_f, $(dw/dt)_{max}$, $(dw/dt)_{mean}$, and W_t. The activation energies of the CC, calculated by the Coats-Redfern method at the heating rates of 5, 10, and 20 °C/min, were 79.08, 76.73, and 75.78 $kJ \cdot mol^{-1}$, respectively. This variation implied that the CC could be decomposed more easily at higher heating rates. The emissions of small-molecule gases during the pyrolysis corresponded well with TG curves.

Being rich in K, P, and Ca, CCA has potential for use as a soil amendment. The high SiO_2 content makes it suitable for silicate ceramics production and implies the potential of CCA for blended cement concrete. The XRF results indicated that the CCA was devoid of toxic metals, suggesting its possibility for clarification. The XRD data revealed potassium, in the form of sylvite, and silica, in the form of quartz, as the two major crystal phases in CCA. The SEM/EDX analysis suggested that large unburnt carbon residue particles exist in CCA. The interior of the agglomerate exhibited a porous structure with many pores. These findings reveal the potential of these carbon residues in CCA as precursor materials for low-cost adsorbent. The interior of the agglomerate was enriched with K and Cl, so the evolution of K was inferred to be mostly in the form of KCl.

ACKNOWLEDGMENTS

The authors are grateful for the support of Rural Energy Comprehensive Construction Found of the ministry of agriculture of China (Grant. No. 2015-36).

REFERENCES CITED

Abraham, R., George, J., Thomas, J., and Yusuff, K. K. M. (2013). "Physicochemical characterization and possible application of the waste biomass ash from oleoresin industries of India," *Fuel* 109, 366-372. DOI: 10.1016/j.fuel.2013.02.067

Adesanya, D. A., and Raheem, A. A. (2009) "A study of the workability and compressive strength characteristics of corn cob ash blended cement concrete," *Construction and Building Materials* 23(1), 311-317. DOI: 10.1016/j.conbuildmat.2007.12.004

Adesanya, D. A., and Raheem, A. A. (2010) "A study of the permeability and acid attack of corn cob ash blended cements," *Construction and Building Materials* 24(3), 403-409. DOI: 10.1016/j.conbuildmat.2009.02.001

Asmadi, M., Kawamoto, H., and Saka, S. (2011). "Thermal reactions of guaiacol and syringol as lignin model aromatic nuclei," *Journal of Analytical and Applied Pyrolysis* 92(1), 88-98. DOI: 10.1016/j.jaap.2011.04.011

Avila-Segura, M., Barak, P., Hedtcke, J. L., and Posner, J. L. (2011). "Nutrient and alkalinity removal by corn grain, stover and cob harvest in Upper Midwest USA," *Biomass and Bioenergy* 35(3), 1190-1195. DOI: 10.1016/j.biombioe.2010.12.010

Baray, G. M. R., Silva, P. M. M., Melendez, Z. M., Gutierrez, J. S., Guzman, V. V., Lopez, O. A., and Collins-Martinez, V. (2014). "Thermogravimetric study on the pyrolysis kinetics of apple pomace as waste biomass," *International Journal of Hydrogen Energy* 39(29), 16619-16627. DOI: 10.1016/j.ijhydene.2014.06.012

Baroni, É. G., Tannous, K., Rueda-Ordóñez, Y. J., and Tinoco-Navarro, L. K. (2016). "The applicability of isoconversional models in estimating the kinetic parameters of biomass pyrolysis," *Journal of Thermal Analysis and Calorimetry* 123, 909-917. DOI: 10.1007/s10973-015-4707-9

Brachi, P., Miccio, F., Miccio, M., and Ruoppolo, G. (2015). "Isoconversional kinetic analysis of olive pomace decomposition under torrefaction operating conditions," *Fuel Processing Technology* 130, 147-154. DOI: 10.1016/j.fuproc.2014.09.043

Cao, Q., Xie, K. C., Bao, W. R., and Shen, S. G. (2004). "Pyrolytic behavior of waste corn cob," *Bioresource Technology* 94(1), 83-89. DOI: 10.1016/j.biortech.2003.10.031

Chirone, R., Miccio, F., and Scala, F. (2004). "On the relevance of axial and transversal fuel segregation during the FB combustion of a biomass," *Energy Fuels* 18(4), 1108-1117. DOI: 10.1021/ef034084j

Chyang, C. S., Duan, F., Lin, S. M., and Tso, J. (2012). "A study on fluidized bed combustion characteristics of corncob in three different combustion modes," *Bioresource Technology* 116, 184-189. DOI: 10.1016/j.biortech.2012.04.041

Du, Z. Y., Sarofim, A. F., and Longwell, J. P. (1990). "Activation energy distribution in temperature-programmed desorption: Modeling and application to the soot oxygen system," *Energy Fuels* 4(3), 296-302. DOI: 10.1021/ef00021a014

Ferdous, D., Dalai, A. K., Bej, S. K., Thring, R. W., and Bakhshi, N. N. (2001). "Production of H_2 and medium bit gas via pyrolysis of lignins in a fixed-bed reactor," *Fuel Processing Technology* 70(1), 9-26. DOI: 10.1016/S0378-3820(00)00147-8

Gao, N. B., Li, A. M., Quan, C., Du, L., and Duan, Y. (2013). "TG–FTIR and Py–GC/MS analysis on pyrolysis and combustion of pine sawdust," *Journal of Analytical and Applied Pyrolysis* 100, 26-32. DOI: 10.1016/j.jaap.2012.11.009

Jensen, A., Dam-Johansen, K., Wojtowicz, M. A., and Serio, M. A. (1998). "TG-FTIR study of the influence of potassium chloride on wheat straw pyrolysis," *Energy Fuels* 12(5), 929-938. DOI: 10.1021/ef980008i

Jiang, X., Li, C., Chi, Y., and Yan, J. (2010). "TG-FTIR study on urea-formaldehyde resin residue during pyrolysis and combustion," *Journal of Hazardous Materials* 173(1-3), 205-210. DOI: 10.1016/j.jhazmat.2009.08.070

Kumar, A., Wang, L. J., Dzenis, Y. A., Jones, D. D., and Hanna, M. A. (2008). "Thermogravimetric characterization of corn stover as gasification and pyrolysis feedstock," *Biomass and Bioenergy* 32(5), 460-467. DOI: 10.1016/j.biombioe.2007.11.004

Kumar, A., Jones, D. D., and Hanna, M. A. (2009). "Thermochemical biomass gasification: A review of the current status of the technology," *Energies* 2(3), 556-581. DOI: 10.3390/en20300556

Li, S., Lyons-Hart, J., Banyasz, J., and Shafer, K. (2001). "Real-time evolved gas analysis by FTIR method: An experimental study of cellulose pyrolysis," *Fuel* 80(12), 1809-181. DOI: 10.1016/S0016-2361(01)00064-3

Liang, X. H., and Kozinski, J. A. (2000). "Numerical modeling of combustion and pyrolysis of cellulosic biomass in thermogravimetric systems," *Fuel* 79(12), 1477-1486. DOI: 10.1016/S0016-2361(99)00286-0

Lin, J. L., Keener, H. M., and Essenhigh, R. H. (1995). "Pyrolysis and combustion of corncobs in a fluidized bed: Measurement and analysis of behavior," *Combustion and Flame* 100(1-2), 271-282. DOI: 10.1016/0010-2180(94)00143-G

Liu, Q., Wang, S. R., Zheng, Y., Luo, Z. Y., and Cen, K. F. (2008). "Mechanism study of wood lignin pyrolysis by using TG–FTIR analysis," *Journal of Analytical and Applied Pyrolysis* 82(1), 170-177. DOI: 10.1016/j.jaap.2008.03.007

Maroto-Valer, M. M., Taulbee, D. N., and Hower, J. C. (1999). "Novel separation of the differing forms of unburned carbon present in fly ash using density gradient centrifugation," *Energy Fuels* 13(4), 947-953. DOI: 10.1021/ef990029s

Mazlan, M. A. F., Uemura, Y., Osman, N. B., and Yusup, S. (2015). "Fast pyrolysis of hardwood residues using a fixed bed drop-type pyrolyzer," *Energy Conversion and Management* 98, 208-214. DOI: 10.1016/j.enconman.2015.03.102

McKendry, P. (2002). "Energy production from biomass (Part 2): Conversion technologies," *Bioresource Technology* 83(1), 47-54. DOI: 10.1016/S0960-8524(01)00119-5

Meng, A. H., Zhou, H., Qin, L., Zhang, Y. G., and Li, Q. H. (2013). "Quantitative and kinetic TG-FTIR investigation on three kinds of biomass pyrolysis," *Journal of Analytical and Applied Pyrolysis* 104, 28-37. DOI: 10.1016/j.jaap.2013.09.013

Munir, S., Daood, S. S., Nimmo, W., Cunliffe, A. M., and Gibbs, B. M. (2009). "Thermal analysis and devolatilization kinetics of cotton stalk, sugar cane bagasse and shea meal under nitrogen and air atmospheres," *Bioresource Technology* 100(3), 1413-1418. DOI: 10.1016/j.biortech.2008.07.065

Pan, H., and Eberhardt, T. L. (2011), "Characterization of fly ash from the gasification of wood and assessment for its application as a soil amendment," *BioResources* 6(4), 3987-4004. DOI: 10.15376/biores.6.4.3987-4004

Rath, J., and Staudinger, G. (2001). "Cracking reactions of tar from pyrolysis of spruce wood," *Fuel* 80(10), 1379-1389. DOI: 10.1016/S0016-2361(01)00016-3

Shim, J., Velmurugan, P., and Oh, B. T. (2015). "Extraction and physical characterization of amorphous silica made from corn cob ash at variable pH conditions via sol gel processing," *Journal of Industrial and Engineering Chemistry* 30, 249-253. DOI: 10.1016/j.jiec.2015.05.029

Sun, Z. A., Shen, J. Z., Jin, B. S., and Wei, L. Y. (2010). "Combustion characteristics of cotton stalk in FBC," *Biomass and Bioenergy* 34(5), 761-770. DOI: 10.1016/j.biombioe.2010.01.019

Tippayawong, N., Tantakitti, C., and Thavornun, S. (2006). "Use of rice husk and corncob as renewable energy sources for tobacco-curing," *Energy for Sustainable Development* 10(3), 68-73. DOI: 10.1016/S0973-0826(08)60546-3

Umamaheswaran, K., and Batra, V. S. (2008). "Physio-chemical characterization of India biomass ashes," *Fuel* 87(6), 628-638. DOI: 10.1016/j.fuel.2007.05.045

Vamvuka, D., and Zografos, D. (2004). "Predicting the behaviour of ash from agricultural wastes during combustion," *Fuel* 83(14-15), 2051-2057. DOI: 10.1016/j.fuel.2004.04.012

Vamvuka, D., Kakaras, E., Kastanaki, E., and Grammelis, P. (2003). "Pyrolysis characteristics and kinetics of biomass residuals mixtures with lignite," *Fuel* 82(15-17), 1949-1960. DOI: 10.1016/S0016-2361(03)00153-4

Vassilev, S. V., Baxter, D., Andersen, L. K., and Vassileva, C. G. (2013). "An overview of the composition and application of biomass ash. Part 1. Phase-mineral and chemical composition and classification," *Fuel* 105, 40-76. DOI: 10.1016/j.fuel.2012.09.041

Wang, L., Hustad, J. E., and Gronli, M. (2012). "Sintering characteristics and mineral transformation behaviors of corn cob ashes," *Energy Fuels* 26(9), 5905-5916. DOI: 10.1021/ef300215x

Wu, C. F., Wang, Z. C., Huang, J., and Williams, P. T. (2013). "Pyrolysis/gasification of cellulose, hemicellulose and lignin for hydrogen production in the presence of various nickel-based catalysts," *Fuel* 106, 697-706. DOI: 10.1016/j.fuel.2012.10.064

Yang, H. P., Yan, R., Chen H. P., Lee, D. H., and Zheng, C. G. (2007). "Characteristics of hemicellulose, cellulose and lignin pyrolysis," *Fuel* 86(12), 1781-1788. DOI: 10.1016/j.fuel.2006.12.013

Yao, X. W., and Xu, K. L. (2015). "Pyrolysis characteristics of corn cob and release rule of gas products," *Transactions of the Chinese Society of Agricultural Engineering* 31(3), 275-282. DOI: 10.3969/j.issn.1002-6819.2015.03.037 (in Chinese)

Yao, X. W., Xu, K. L., and Li, Y. (2016). "Physicochemical properties and possible applications of waste corncob fly ash from biomass gasification industries of China," *BioResources* 11(2), 3783-3798. DOI: 10.15376/biores.11.2.3783-3798

Yao, X. W., and Xu, K. L. (2016). "Comparative study of characterization and utilization of corncob ashes from gasification process and combustion process," *Construction and Building Materials* 119, 215-222. DOI: 10.1016/j.conbuildmat.2016.04.077

Youssef, M. A., Wahid, S. S., Mohamed, M. A., and Askalany, A. A. (2009). "Experimental study on Egyptian biomass combustion in circulating fluidized bed," *Applied Energy* 86(12), 2644-2650. DOI: 10.1016/j.apenergy.2009.04.021

Zhang, Z. P., He, C., Sun, T. L., Zhang, Z., Song, K. L., Wu, Q. L., and Zhang, Q. G. (2016). "Thermo-physical properties of pretreated agricultural residues for bio-hydrogen production using thermo-gravimetric analysis," *International Journal of Hydrogen Energy* 41(10), 5234-5242. DOI: 10.1016/j.ijhydene.2016.01.079

Article submitted: July 3, 2016; Peer review completed: September 22, 2016; Revised version received and accepted: September 22, 2016; Published: September 29, 2016.
DOI: 10.15376/biores.11.4.9823-9841